PHYSICAL REVIEW B VOLUME 27, NUMBER 10 15 MAY 1983

Anisotropic phonon-dislocation scattering in deformed LiF

G. A. Northrop, E. J. Cotts, A. C. Anderson, and J. P. Wolfe
Department of Physics and Materials Research Laboratory, University of Illinois at Urbana-Champaign, Urbana, Illinois 61801
(Received 20 December 1982)

By direct imaging of ballistic phonons having equivalent temperatures near 4 K in LiF, we have found that a subset of fast-transverse phonons can propagate without scattering even in heavily deformed samples. The highly anisotropic phonon-scattering cross section is consistent with the concept of fluttering dislocations. The magnitude of the scattering cross section has been obtained for the first time. For small plastic deformation the measured cross section agrees with that calculated theoretically using a measured dislocation density. However, at large deformation the calculated cross section is too small, supporting the speculation that a larger density of dislocation dipoles may provide the dominant scattering. Also consistent with the concept of fluttering dislocations, γ irradiation reduces the phonon scattering created by deformation, presumably by pinning of the dislocations. It is demonstrated that the method of phonon imaging used here provides details of phonon scattering processes which are not available from conventional thermal-transport measurements, especially when the scattering is anisotropic.

I. INTRODUCTION

Lithium fluoride was used by Johnston and Gilman[1] in their classical investigation of dislocations. It was natural, therefore, that LiF should later be used in several studies of the phonon-dislocation interaction in thermal transport.[2–8] From these studies a simple picture, as described later, has evolved to explain the thermal conductivity κ of deformed LiF at temperatures below ~ 1 K. At higher temperatures, however, the scattering mechanisms are still in doubt. In this paper[9] we provide detailed information on phonon scattering processes at temperatures $T \gtrsim 1$ K using a ballistic phonon imaging technique[10] which resolves both phonon polarization and direction of propagation.

Two basic scattering mechanisms have been proposed for the phonon-dislocation interaction. The first is a static mechanism which involves an anharmonic coupling between the strain fields of the phonon and those of a sessile dislocation.[11,12] The second envisions a resonant interaction between a phonon of frequency ω and a dislocation segment of length L vibrating or "fluttering" at the phonon frequency.[13,14] The length L is the distance between two pinning points. The resonant frequency of the segment is $\omega \approx \pi \bar{v}/L$, where $\bar{v}$ is a mean phonon velocity. For phonons having frequencies near the dislocation resonant frequency, the fluttering mechanism is the dominant scattering process. The pinning points are statistically distributed, resulting in a broad spectrum of resonant frequencies.

The following experimental evidence suggests that the fluttering mechanism is the most important scattering process in plastically deformed LiF crystals at temperatures below ~ 1 K.

(i) The magnitude of the scattering is too large to be explained by the static mechanism.[6,7]

(ii) Thermal conductivity and ballistic-phonon measurements indicate that the slow-transverse mode is scattered most strongly by the dislocations,[6] and it is this mode which would be expected to excite a fluttering dislocation in LiF. The fast-transverse phonons are so weakly perturbed by dislocations that they scatter primarily at the surfaces of the sample. This accounts for the T^3 dependence of κ ("boundary scattering"),[6] for the dependence of κ on sample dimensions even in heavily deformed samples,[7,8] and for the fact that κ is only weakly dependent on the density of dislocations present.[6,7]

(iii) Exposure of deformed samples to γ irradiation does not remove the dislocations but does restore the thermal conductivity to predeformation values.[6–8] This restoration occurs first at the lowest temperatures and continues to higher temperatures with progressive γ irradiations. This is the expected behavior for the fluttering mechanism since pinning of the dislocations by radiation-induced defects reduces L, thereby increasing the resonant frequency. The result is to decrease the scattering cross section for the low-frequency phonons which are the major heat carriers at the lower temperatures.

Thus the model of fluttering dislocations is consistent[7,14] with the measured κ at $T < 1$ K. Howev-

er, thermal conductivity measurements are a poor test of the details of this theory since the thermal conductance is dominated by phonons *not* scattered by dislocations. In effect, the desired information about the phonon-dislocation interaction is masked.

At temperatures above 1 K the situation appeared to change. Experimentally the γ irradiations[7,8] were much less effective in restoring κ to predeformation values, and all phonon modes were scattered.[8] Yet it appeared that some subset of phonons still had a mean free path of order 1 cm even in heavily deformed samples, since κ was still dependent on sample dimensions. In addition the theory of fluttering dislocations could not explain the strong scattering observed at $T \gtrsim 1$ K without assuming a larger density of dislocations in the form of dipoles.[14] This conclusion is compatible with the experimental results because dipoles do not appear in the experimental etch-pit counts used to obtain the density of dislocations.[1,6,7]

Since some phonons have a mean free path of order 1 cm, we have used a ballistic-phonon-imaging apparatus for a detailed study of phonon scattering in deformed LiF at temperatures $\gtrsim 2$ K. The temporal and angular resolution of the technique allows the identification of the phonon mode, polarization, and direction of propagation. Intensity resolution provides a transmission coefficient or phonon mean free path. The technique and results are presented in Sec. II, and a comparison with theory is discussed in Sec. III. In brief, the strong phonon scattering anisotropy predicted for the fluttering mechanism is observed, and a significant decrease in scattering with γ irradiation does occur in deformed LiF for temperatures near 4 K. In the process, we have developed a method for quantifying the phonon-dislocation scattering mechanism via changes the scattering produces in phonon-focusing structures. We expect that the general technique will be adaptable to the study of interaction of phonons with other defects in crystals.

II. TECHNIQUES AND RESULTS

A block diagram of the ballistic-phonon-imaging technique[10,15,16] is shown in Fig. 1. The light beam from a cw Nd:YAG (YAG is yttrium aluminum garnet) laser is chopped by an acousto-optic (AO) coupler and focused to a point on one surface of a sample immersed in liquid ^{4}He. The focused pulse can be rastered through a 256×256 position matrix on the sample surface. This surface is coated with a constantan film to absorb the laser pulses. An absorbed pulse heats the film locally and thence radiates thermal phonons into the sample. For typical laser powers, the phonons have an equivalent temperature of ~ 4 K. An Al superconducting bolometer on the opposite surface detects the ballistic phonons. The signal is amplified and integrated during a time gate, which provides the temporal resolution. This time-of-flight information assists in the identification of phonon mode and polarization. The signal is stored in a computer, which then instructs the mirrors to move the following laser pulse to the next point in the 256×256 position rastor on the metalized surface of the sample. Repositioning of the source of the heat pulse provides the angular resolution in this technique and, with knowledge of the sample thickness, identifies the direction of propagation of the detected phonons. The intensity pattern stored in the computer provides a profile of relative intensities for the directions of propagation scanned during the measurement. In discussing this pattern it is useful to invoke reciprocity, i.e., to think of the phonons as originating at the detector and being recorded by the 256×256 point rastor on the metalized surface.

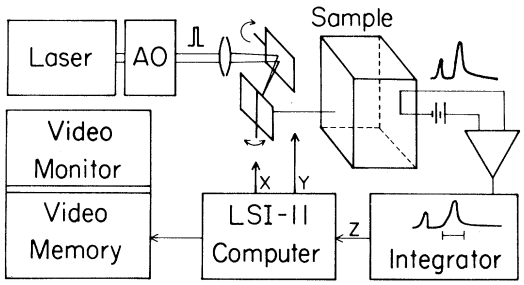

FIG. 1. Block diagram of the ballistic-phonon-imaging apparatus. The components are discussed in the text and in Ref. 15. In the present work, the laser and acousto-optic coupler typically produce 180-ns, 0.5-watt pulses at a 50-kHz rate.

Three LiF samples with (100) faces were cut from $0.7\times0.7\times5$ cm^3 pieces of the same material used in Ref. 8. One piece was not deformed, one was deformed under compression by 1.6% to introduce dislocations, the third piece was deformed 10%. One ballistic-phonon sample was cut from each of these pieces, with lengths of 0.45, 0.35, and 0.44 cm, respectively. For convenience, we will refer to these as the 0%, 1.6%, or 10% samples. A diagram of sample deformation is shown in Fig. 2. Compression along [100] produced expansion primarily along [010] as the [001] dimension was partly constrained by the deformation jig. Since LiF tends to form slip planes[17] of the $\{110\}$ type with Burgers vectors along $\langle 1\bar{1}0\rangle$, the most likely slip planes in these samples are (110) and $(1\bar{1}0)$ containing edge and screw dislocations oriented as shown in Fig. 2(a).

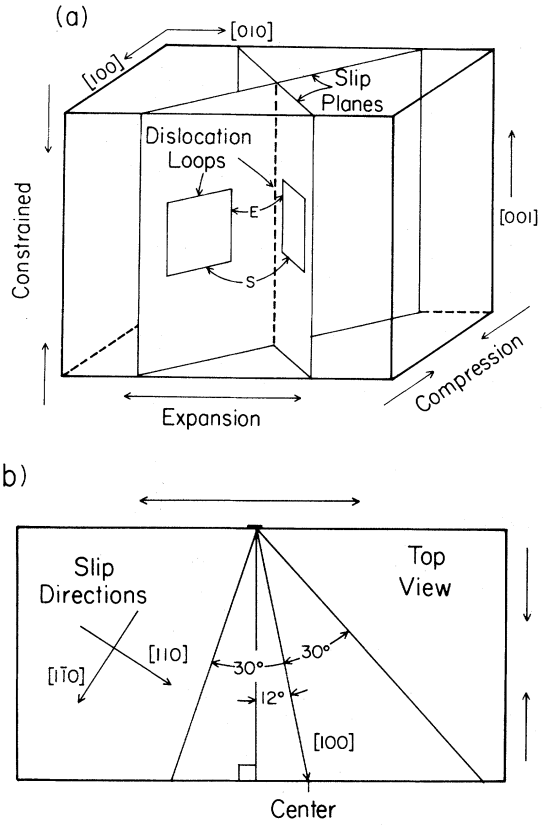

FIG. 2. Sample geometry of the deformed LiF samples. (a) E denotes edge dislocations; S denotes screw dislocations. (b) Reorientation of the [100] direction relative to the sample face for the sample deformed by 10%. (The 30° angles correspond to the position at which the horizontal ridge in Fig. 11 was scanned.)

Deformation also produced a rotation of the [100] crystallographic axis relative to the face of each sample. The 12° rotation for the 10% sample is shown in Fig. 2(b).

The (100) faces of the samples were polished with 0.3-μm alumina suspended in ethanol. A 2400-Å layer of constantan was vapor deposited on one of these surfaces, and a 700-Å Al bolometer on the opposite face. The bolometers had a sensitive area of 2×10^{-2} cm on a side (5×10^{-3} cm for the thinner sample compressed by 1.6%).

After measurements were obtained on these three samples, the 10% sample was exposed to 6×10^{5} rad of γ irradiation, remeasured, exposed to an accumulated dose of 6×10^{6} rad, and measured again. (1 rad = 100 ergs/g.) The purpose was to study the effect of pinning on the phonon-dislocation interaction as discussed in Sec. I.

The ballistic-phonon images obtained for the three samples are shown in Figs. 3–5. Part (a) of each figure shows the measured intensity profile, while part (b) provides the same information in a three-dimensional plot provided by the computer. The amplifier gate was set to accept transverse-acoustic phonons propagating ballistically across the sample. In Fig. 3 the fast-transverse mode produces the large, sharp horizontal and vertical "ridges" in the intensity profile for the undeformed sample. The slow-transverse mode produces diagonal "ramps" which are difficult to see except where they overlap to form the intense diamond at the center of Fig. 3(a).

The concentration of the phonon energy flux in certain directions, as shown in Fig. 3, stems from the elastic anisotropy of crystals[10,15,18] and is referred to as phonon focusing. Phonon focusing is a well understood effect, and arises because phonons need not propagate in the same direction as their wave vector. Since the formation of intense focusing structures depends upon direct propagation of phonons from source to detector, any phonons scattered in the bulk of the crystal cannot contribute to these structures. The structure is strongly suppressed if the focusing direction is coincidentally a direction of strong scattering for a defect having an anisotropic scattering cross section.

The changes seen in Figs. 4 and 5, relative to Fig. 3, result from phonon scattering introduced by deformation. The most obvious changes in the 10% sample of Fig. 5 are the suppression of all of the slow-transverse signal and one of the fast-transverse ridges. (The longitudinal mode, which displays no sharp structure, was also suppressed by deformation.) Figure 6 shows additional changes produced by γ irradiation.

The bright ridges in the ballistic-phonon images of the deformed samples, Figs. 4 and 5, correspond to ballistic propagation as for the undeformed crystal, Fig. 3. This is evidenced in the temporal domain by a well-defined heat pulse traveling at the speed of sound. But it is found that only a fraction of the phonons produced at the metal film propagate ballistically across the deformed crystal. The remaining scattered phonons traverse the sample diffusively, resulting in a broad pulse arriving at the detector later than the ballistic delay time. Figure 7 shows the bolometer signal as a function of time for three laser positions on the 10% sample. The first pulse in all of the traces is due to a small amount of scattered laser light striking the bolometer directly, and serves to mark $t=0$. For trace 7(a) the laser was positioned on the horizontal ridge of Fig. 5 resulting in an intense ballistic pulse with a long tail. For curve 7(b) the laser was moved to a point on the edge of the horizontal ridge. There the ballistic por-

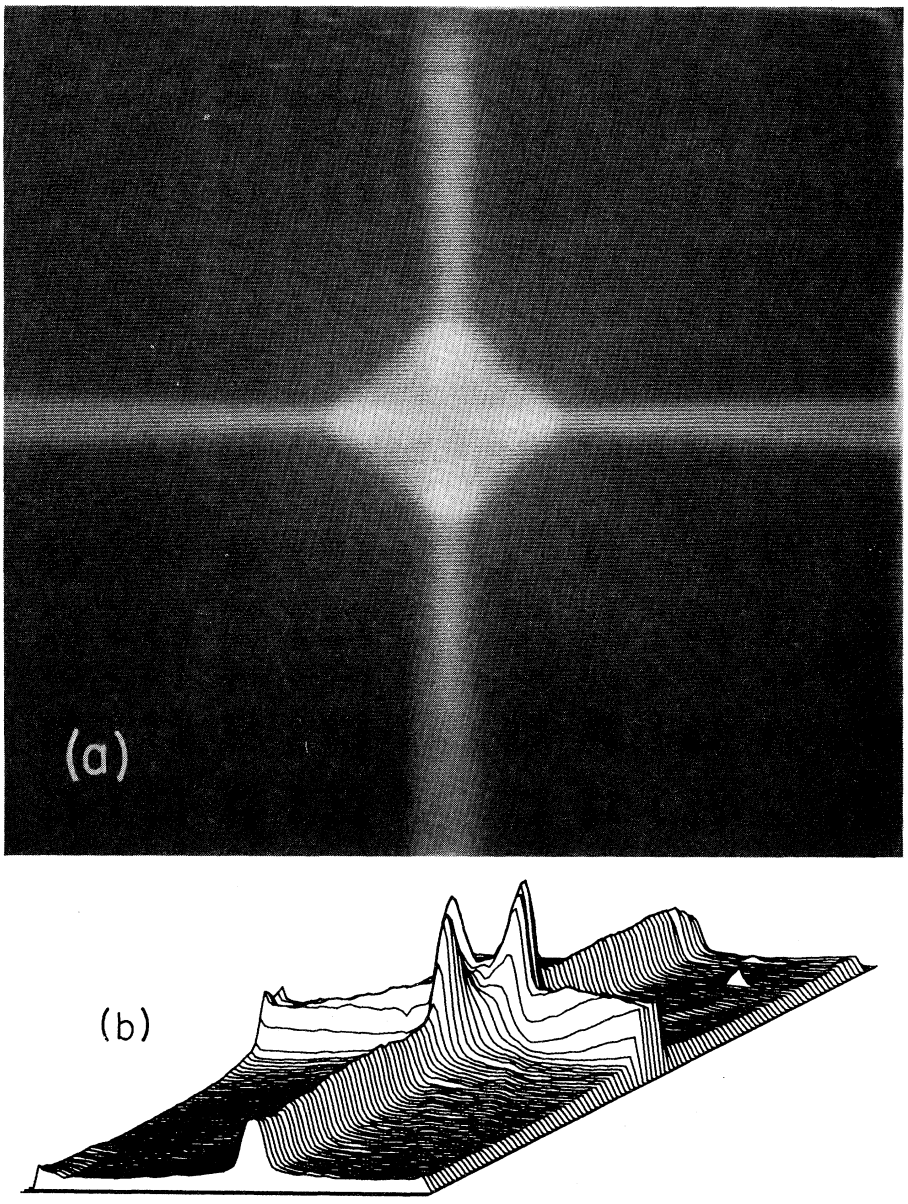

FIG. 3. (a) Ballistic-phonon image of the undeformed sample of LiF. The center corresponds to exact [100] propagation and the image extends to about 38° from the [100] axis at the edges. The brightness is proportional to the detected phonon intensity, and the anisotropy is due to phonon focusing. (b) Intensity profile of information in (a).

tion is dramatically reduced, but the tail is basically unchanged. The third trace 7(c), taken at a point below the ridge, shows no ballistic character, and reveals the tail from 7(a) to be a broad delayed pulse. The delay time for the maximum in intensity of this broad pulse varies from 3 to 5 times the ballistic delay, and the intensity shows no large variation from point to point on the sample.

This dual nature of phonon transport in the 10% sample may also be observed in a set of images taken at various times after the laser pulse. For a delay of about 1 μs, Fig. 5 shows the large ballistic intensity in the horizontal ridge, with little intensity in other areas. Images taken at delays of 2, 3, 5, and 8 μs are plotted in Fig. 8, and show a rapid decrease of the ridge intensities at times greater than the 1-μs

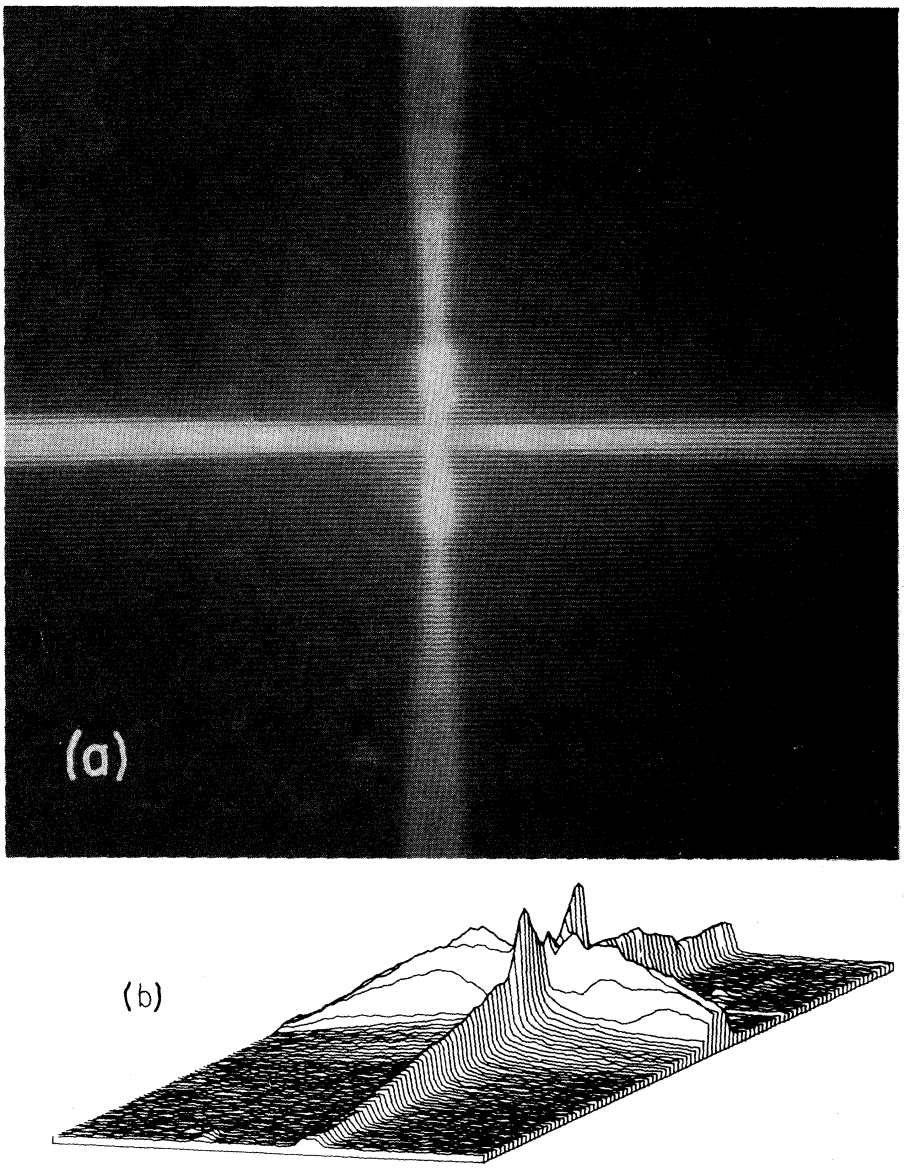

FIG. 4. (a) Ballistic-phonon image of the sample deformed by 1.6%. The viewing direction is along the direction of compression; the lateral expansion occurred in the horizontal direction in this figure. The intensity scale is arbitrary and cannot be compared directly with Figs. 3 or 5. (b) Intensity profile of information in (a).

ballistic time of flight. In other areas of the image the intensity increases and reaches a maximum at around 4 μs, characterizing the diffusive portion of the thermal transport. The transition from ballistic to diffusive is not sudden. The ballistic-phonon-focusing pattern decreases in intensity and broadens spatially with increasing delay time. The remnant of the sharp focusing pattern is probably due to phonons which scatter a few times near the source until they reach a direction having a low scattering cross section, where they then propagate ballistically to the detector.

In summary, we have observed in deformed samples of LiF two variations of thermal transport: (1) ballistic transmission of a fraction of the phonons through an angular window of minimal scattering, and (2) diffusive transport of all other phonons. A phonon image taken at ballistic delay times, on a de-

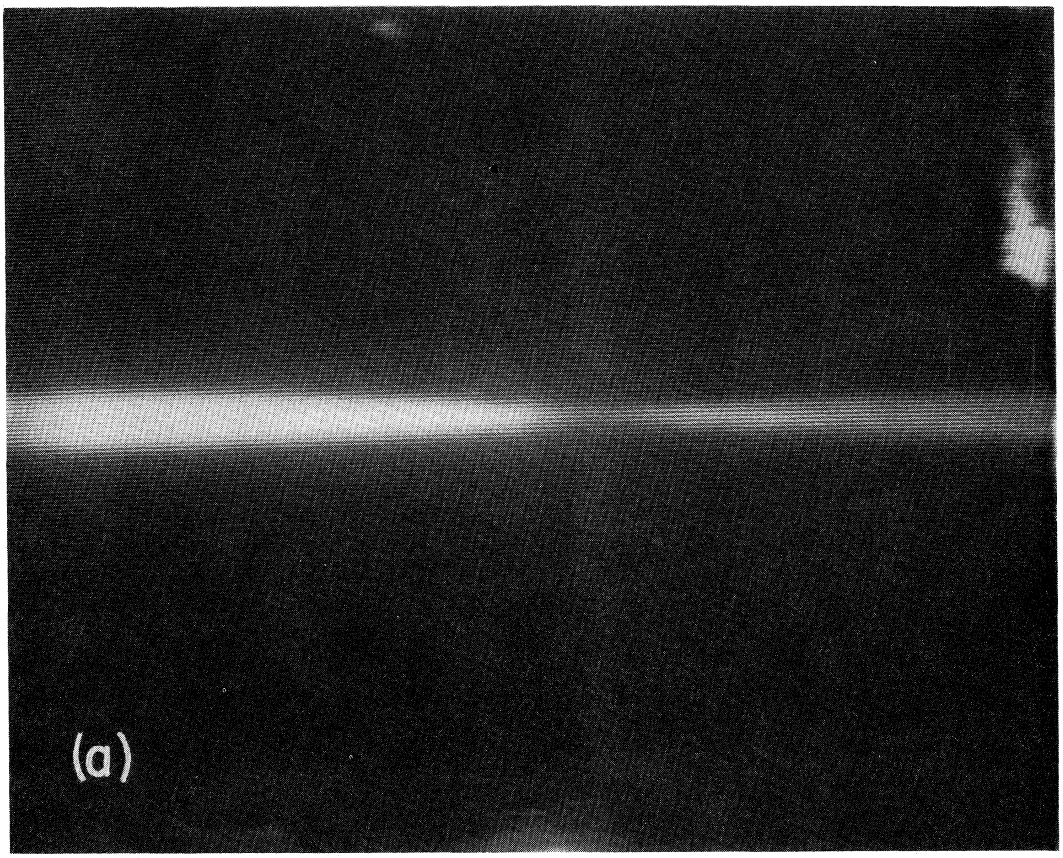

FIG. 5. Ballistic-phonon image of the sample deformed by 10%. Note the partial attenuation of the vertical ridge of the fast-transverse mode and the total attenuation of the slow-transverse mode. The dim vertical ridge may be difficult to see in (a), but it is evident in the intensity profile of (b). The fact that the intersection of the ridges is off center and that the horizontal ridge is most intense on the left is due to the reorientation of the [100] axis during deformation, as shown in Fig. 2(b). (The dip in intensity near the left end of the horizontal ridge is due to a defect in the constantan film.)

formed sample, when compared to a similar image for a nondeformed sample, provides an indication of the angular dependence of the scattering anisotropy. In the following section we compare our results with the model of fluttering dislocations.

III. ANALYSIS

Only the model of fluttering dislocations[14] will be discussed since this model predicts a strong anisotropy in the phonon scattering cross section, an an-

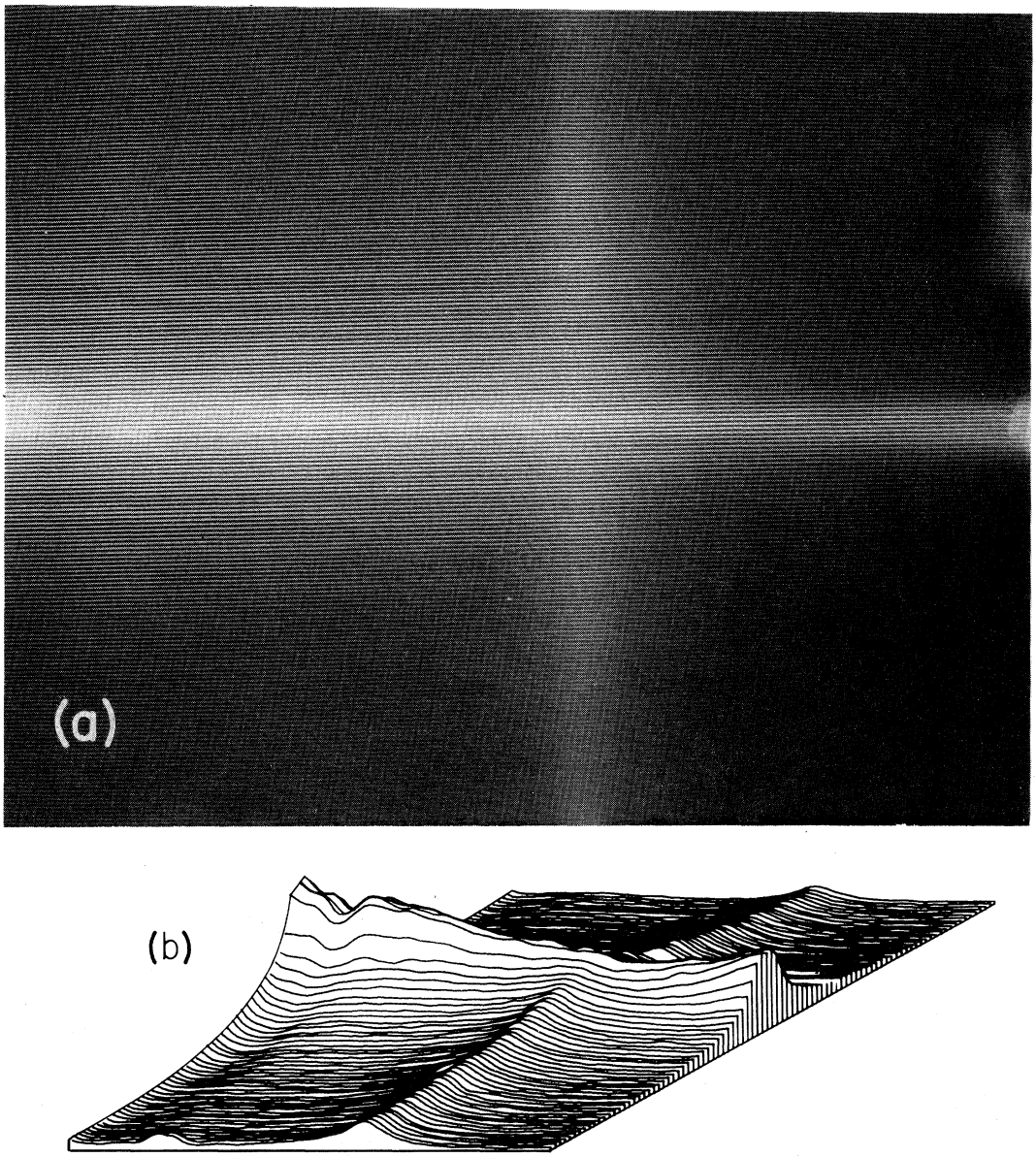

FIG. 6. Ballistic-phonon image (a) and intensity profile (b) of the 10% sample after exposure to 6×10^6 rad of γ irradiation. Note the increase in intensity of the vertical ridge relative to the horizontal ridge, compared to that in Fig. 5. Also the width of the ridge structure has increased due to scattering by defects introduced by γ irradiation.

isotropy which is observed in the present ballistic-phonon measurements. Predictions of the model will be compared to measurements for which the time gate is set to register only nonscattered phonons. Phonons that scatter one or more times travel farther than the line-of-sight path from source to detector and arrive after the time gate. In this approximation the observed phonon intensity is

$$I(\theta,\phi)=I_0(\theta,\phi)e^{-d/l(\theta,\phi)}, \quad (1)$$

where $I_0(\theta,\phi)$ is the anisotropic intensity due to phonon focusing, d is the distance between source and detector, and $l(\theta,\phi)$ is the angle-dependent phonon mean free path. Since the undeformed sample exhibits primarily ballistic propagation, it should be described by $I=I_0(\theta,\phi)$.

The mean free path $l(\theta,\phi)$ has been calculated by Kneezel and Granato.[14] The phonon shear-stress component σ_0, which lies across the glide plane and along the Burgers vector $\vec{b}$ of a dislocation, pro-

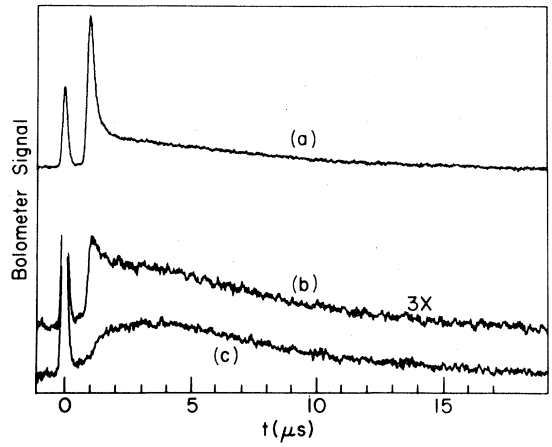

FIG. 7. Bolometer signal as a function of time for three positions on the 10% sample: (a) on the horizontal ridge, 30° from the [100] center in Fig. 5(a); (b) still at 30°, but just on the bottom edge of the horizontal ridge; (c) continuing downward to a point well below the horizontal ridge. In (b) and (c) the signal is amplified by a factor of 3.

duces a force $b\sigma_0$ per unit length on the dislocation. The equation of motion for the dislocation is that of a damped, infinite string of mass A, damping constant B, and tension C, which is forced to oscillate by the spatially and temporally oscillating phonon strain field:

$$A\frac{d^2y}{dt^2}+B\frac{dy}{dt}-C\frac{d^2y}{dt^2}=b\sigma_0\cos(kx-\omega t)\ . \quad (2)$$

A solution to this equation is a traveling wave on the dislocation having a frequency ω, and with both in-phase and out-of-phase components. The portion of this solution which is out-of-phase with the forcing term on the right-hand side of Eq. (2) is proportional to the damping B, and results in a dispersal of phonon energy by the dislocation. The associated inverse phonon mean free path is

$$l^{-1}=\frac{\Omega\Lambda Gb^2s}{v\omega A[(R^2-1)^2+s^2]} \quad (3)$$

where $\Omega=(\sigma_0/\sigma_p)^2$, $s=B/A\omega$, and $R=(C/Av)\sin\eta$. Here Λ is the dislocation density, G is an appropriate elastic constant for the phonon of phase velocity v, σ_p is the total phonon stress, and η is the angle between the dislocation and the phonon wave fronts. When the parameters A and B are evaluated,[14] the ratio s is found to be a constant of order unity.

Two quantities in Eq. (3) produce an anisotropy in the scattering, the resolved shear-stress factor Ω, and the phonon-dislocation angle η. The denominator in Eq. (3) produces a resonant scattering at the angle η_0 for which $R=1$. This resonance, called the Ninomiya resonance,[19] occurs when the component of the phonon wave vector along the dislocation matches the wave vector of the traveling wave on the dislocation. Of the two anisotropic effects, Ω is the most important and is the only one evidenced in the phonon-image data. Reasons for the apparent absence of the Ninomiya resonance will be discussed later. Since the Ninomiya resonance is not observed, we have set the quantity $s[(R^2-1)^2+s^2]^{-1}$ equal to unity for convenience of computation.

The resolved shear-stress factor Ω is a measure of the coupling of a phonon to the allowed motion of a dislocation. It is the same for both screw and edge dislocations, and is a function of the phonon mode, wave vector, and slip plane in which the dislocation

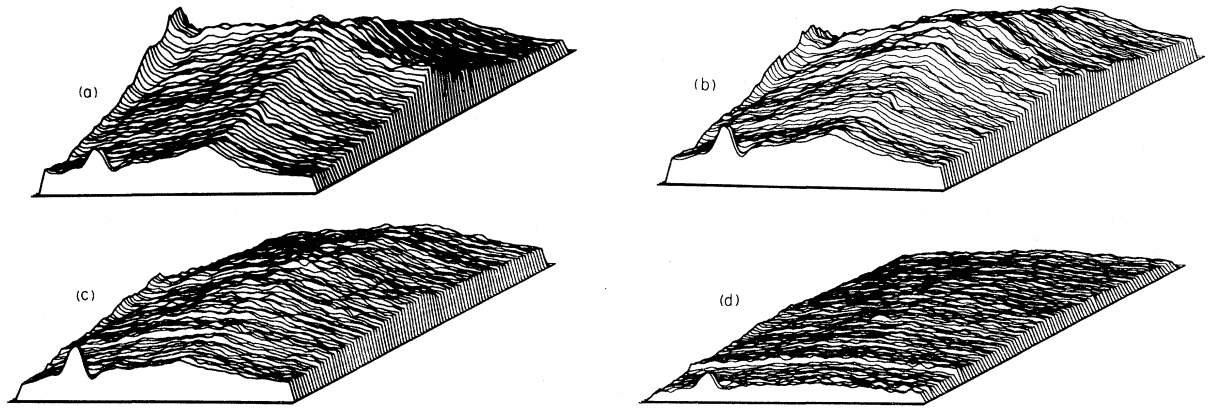

FIG. 8. Sequence of post-ballistic images for the 10% sample. (The image for a ballistic delay time of 1 μs is shown in Fig. 5.) (a) 2 μs; (b) 3 μs; (c) 5 μs; (d) 8 μs.

lies. All that is required to calculate Ω is the phonon stress as a function of wave vector and mode, and this may be obtained from the plane-wave solutions to the equation of motion of the crystal.[16,20] Because of the deformation observed for our samples (see Sec. II), we assume for now that only the (110) and (1$\bar{1}$0) slip systems were activated. The resolved shear stress for these planes is $(\sigma_{11}-\sigma_{22})/2$, where subscripts refer to Cartesian coordinates aligned with the cubic crystalline axes. This may be derived by rotating σ_0 into a [110], [1$\bar{1}$0], [001] coordinate system and taking the resulting σ_{12} component as the resolved shear stress. For plane waves in cubic crystals the strain tensor may be written as[20]

$$e_{lm}=\frac{\partial u_l}{\partial x_m}=i\epsilon_l k_m e^{i(\vec{k}\cdot\vec{x}-\omega t)}, \tag{4}$$

where $\vec{u}$ is the displacement, $\vec{k}$ is the wave vector, and $\vec{\epsilon}$ is the polarization vector. Averaging the square of the resolved shear over the length of the dislocation and using $\sigma_{ij}=C_{ijlm}e_{lm}$ reduced for the case of cubic symmetry, the resolved shear-stress factor may be expressed as

$$\Omega=\left[\frac{\sigma_{11}-\sigma_{22}}{2\,\mathrm{tr}(\sigma)}\right]^2=(\epsilon_1 n_1-\epsilon_2 n_2)^2 \tag{5}$$

where $n_i=k_i/k$ are the components of the unit wave vector. This expression is normalized such that Ω ranges from 0 to 1, which corresponds to the range of no-phonon-dislocation coupling to all of the phonon stress acting upon the dislocation. From Eq. (5) it is clear that minimal scattering should occur when $\sigma_{11}=\sigma_{22}$, which will occur, for example, when $\vec{k}$ or $\vec{\epsilon}$ are parallel to [001].

To emphasize the role of Ω, we rewrite Eq. (1) in the form

$$I(\theta,\phi)=I_0(\theta,\phi)e^{-\beta\Omega(\theta,\phi)}. \tag{6}$$

The constant β, which will be called the scattering strength, includes all of the isotropic factors from Eq. (3) and the length of the sample. The anisotropic factors are contained in Ω. Figure 9 shows contours of constant Ω for LiF in the plane of wave-vector directions corresponding roughly to that appearing in the phonon images. The vertical-horizontal asymmetry results from our assumption that only the (110) and (1$\bar{1}$0) slip planes were activated during deformation. The fraction of phonons transmitted ballistically is approximately the fraction of the (θ,ϕ) angular space for which $\beta\Omega<1$, where β is proportional to the dislocation density and for now will be used as a fitting parameter. To calculate the expected real-space intensity profile, we have used a Monte-Carlo method which generates 4×10^5 randomly oriented $\vec{k}$ vectors and, for each, computes the group-velocity direction, polarization, resolved shear-stress factor, and probability of scattering. The ballistically transmitted phonons are then projected along the group-velocity direction onto the appropriate sample geometry (in-

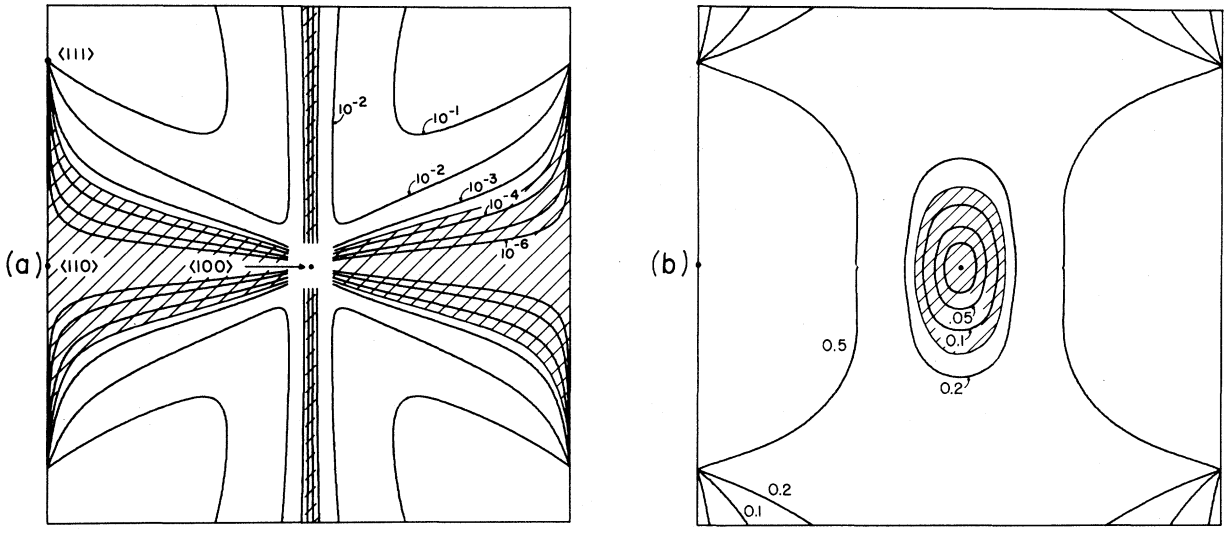

FIG. 9. Contours of constant Ω in wave-vector angle space for LiF deformed as in Fig. 2. (a) Fast-transverse mode. Phonons in the cross-hatched area are transmitted through the 10% sample as discussed in the text. (b) Slow-transverse mode. Phonons in the cross-hatched portion are transmitted through the 1.6% sample, along with most of the fast-transverse mode.

cluding the rotation of the [100] axis, Sec. II) and compiled in a 256×256 image matrix. Some results are shown in Fig. 10, where the factor β of Eq. (6) has been selected so that the computed intensity profiles approximate the measured profiles. The factor β is the *only* adjusted parameter.

For a large density of dislocations, such as occurs in the 10% deformed LiF crystal, β is large and only phonons for which $\Omega\approx0$ can propagate across the entire crystal without scattering. These are the phonons which appear in the ballistic-phonon image of Fig. 5. The condition $\Omega\approx0$ is satisfied in certain angular regions, and then primarily for the fast-transverse mode. Since only a small fraction of the longitudinal- and slow-transverse phonons give $\Omega\approx0$, the following discussion will pertain to the fast-transverse mode alone.

For the fast-transverse mode all $\vec{k}$ that lie in the (001) plane have a polarization $\vec{\epsilon}$ parallel to [001]. Thus $\epsilon_1=\epsilon_2=0$, and $\Omega=0$ for these wave vectors which form the bright horizontal ridge in Fig. 5. For all $\vec{k}$ in the (010) plane, $\vec{\epsilon}$ is parallel to the [010] direction. Hence $\epsilon_1=0$ and $k_2=0$, which again leads to $\Omega=0$. This group of weakly scattered phonons forms the dim vertical ridge in Fig. 5. Since only relative intensities are measured experimentally, the remainder of this discussion will focus on the difference between the horizontal and vertical ridges.

The plots of Fig. 11 are computed phonon intensi-

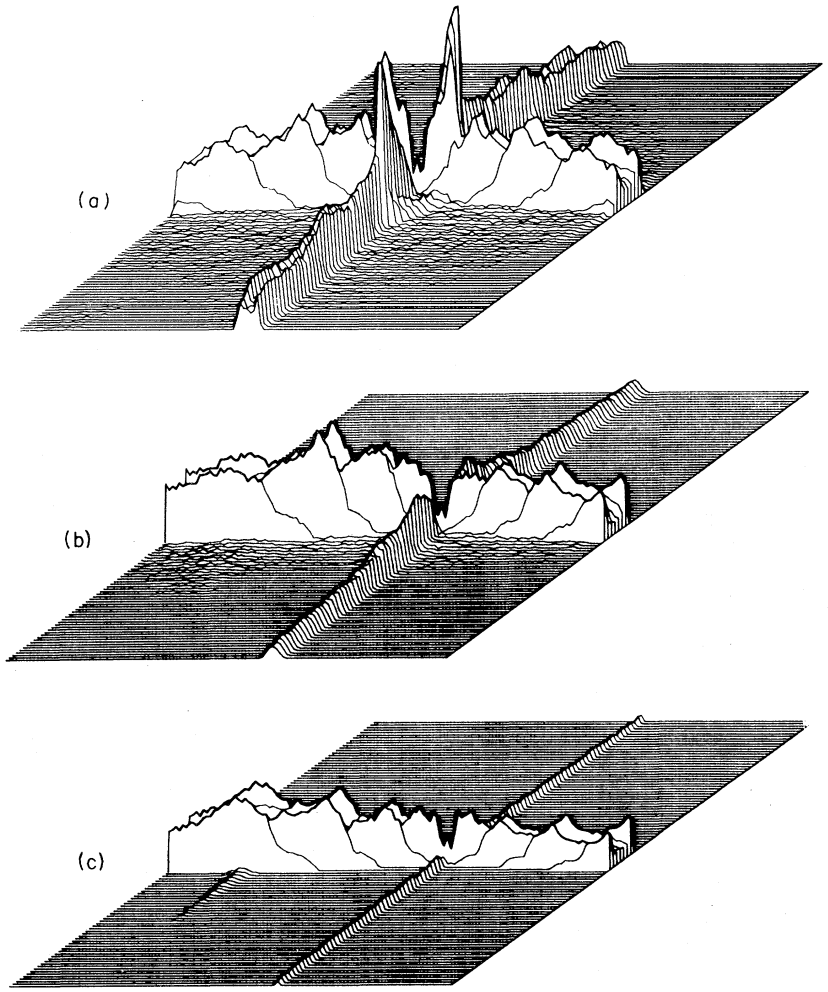

FIG. 10. Monte Carlo computed images, including both transverse modes. (a) 1.6% sample, $\beta=7$ (cf. Fig. 4); (b) 10% sample following 6 Mrad of γ irradiation, $\beta=55$ (cf. Fig. 6); (c) 10% sample not irradiated, $\beta=2800$ (cf. Fig. 5). The crystal-axis rotation, produced by deformation, is included in this computation and causes the increased intensity at the left side of the horizontal ridge.

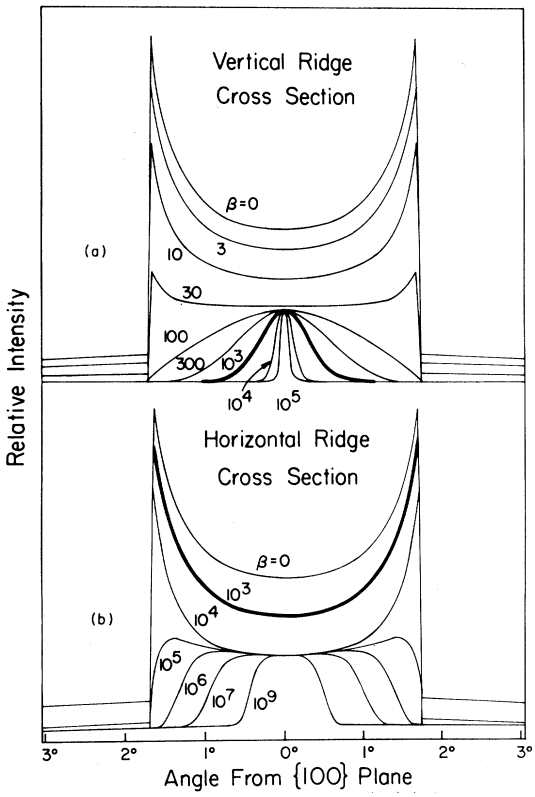

FIG. 11. Calculated phonon intensity near the (a) (010) and (b) (001) planes, including both phonon focusing and dislocation scattering, for several values of β. The heavy lines indicate the expected vertical and horizontal ridge intensities for $\beta=10^3$, which is close to the value of $\beta=2800$ for the 10% sample.

ties for scans perpendicular to the horizontal and vertical ridges at points 30° from the [100] axis [see Fig. 2(b)]. They represent transmitted intensity as a function of angle across each ridge. The symmetric double peaks are phonon-focusing singularities which occur at about 2° on either side of the {100} planes in LiF. The intensity at any point between these singularities is due to the combined contributions of three distinct $\vec{k}$ vectors, whereas points outside the intense ridge correspond to only one $\vec{k}$ vector. (This is due to the folded structure of the group-velocity surface.) The resolved shear-stress factor Ω is exactly zero for $\vec{k}$ in the {100} planes and increases in magnitude as the $\vec{k}$ vector leaves the plane. For $\beta=0$ in Eq. (6) the intensity across the ridge is just $I_0(\theta,\phi)$. The transmitted phonons form bands in $\vec{k}$ space which are centered about the {100} planes and narrow as β increases, since those phonons with $\vec{k}$ vectors furthest from the {100} plane have the greatest probability of being scattered (see Fig. 9). As such a transmission band narrows, the portions outside the singularities in Fig. 11 are the first attenuated, next come two of the $\vec{k}$ vectors in the midportion, followed by the folds at the singularities, until only a narrow portion is left with $\vec{k}$ very nearly in the symmetry plane.

The plots shown in Fig. 11 suggest that a value for β may be obtained by comparing the data from a ballistic-phonon image with the theoretical $I(\theta,\phi)$. This was not a practical approach in our experiments because the angular resolution of the imaging experiment was not high enough to accurately fit the calculated curves in Fig. 11. However, β can be determined by the ratio of total integrated intensity across the horizontal ridge to that across the entire vertical ridge. For such a comparison we have integrated the *theoretical* curves and have plotted, in Fig. 12, the total ridge intensity as a function of β for both the horizontal and vertical ridges. For large β, the integrated intensities exhibit a weak power dependence on β, with the horizontal ridge intensity (H) being proportional to $\beta^{-1/6}$, and the vertical ridge integrated intensity (V) being proportional to $\beta^{-1/2}$. As β approaches 0, both H and V are limited to the same nonattenuated magnitude I_0.

Since the H and V intensities have different dependencies upon β, the β for a *measured* H/V ratio may be determined from the information contained in Fig. 12. The four vertical lines in Fig. 12 represent the H/V ratios taken from our measurements, their position on this plot results in the following values for β. For the 10% sample the measured H/V ratio in Fig. 5 is 20. This ratio, labeled

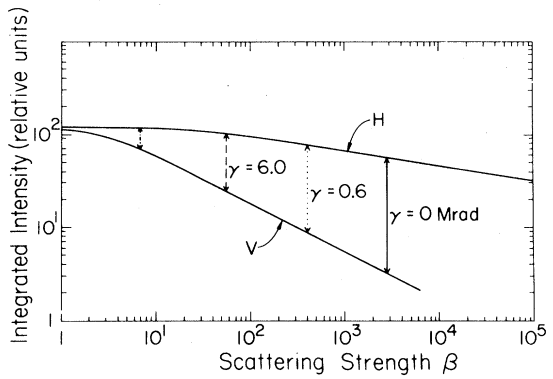

FIG. 12. Integrated horizontal (H) and vertical (V) ridge intensities as a function of β. The H/V ratios measured in phonon images are shown as vertical lines: solid line, 10% deformed sample, with no irradiation; dotted line, 10% sample, 0.6 Mrad; dashed line, 10% sample, 6.0 Mrad; dotted/dashed line, 1.6% deformed sample, no irradiation.

$\gamma=0$ Mrad in Fig. 12, gives $\beta=2800$. After exposure to 0.6 Mrad of γ irradiation the H/V ratio has changed such that $\beta=400$. After a total exposure to 6.0 Mrad (Fig. 6), we find $\beta=55$. Thus each successive dose of irradiation decreased the scattering strength of the dislocations by a factor of ~ 7. The ratio $H/V=1.7$ obtained for the 1.6% sample (Fig. 4) yields $\beta=7$.

Only two deformed samples have been studied, but it is clear that the scattering strength of the dislocation system is a superlinear function of the strain. An increase of 6 in strain resulted in a 400-fold increase in scattering strength between in 1.6% and 10% samples.

Having obtained values for the scattering parameter β which bring the theory into agreement with our measurements, we can look again at the anisotropy of the phonon-dislocation scattering process shown in Fig. 9. In Fig. 9(a) the cross-hatched area (for $\Omega < \frac{1}{2800}$) indicates the angular space within which ballistic propagation of fast-transverse phonons can occur for then 10% sample before irradiation. Likewise in Fig. 9(b), the cross-hatched area (for $\Omega < \frac{1}{7}$) shows the angular region in which slow-transverse phonons can propagate in the 1.6% sample. This transmission, plus phonon focusing, accounts for the two sharp maxima seen in Fig. 4 near the center of the vertical ridge. The two maxima are the upper and lower corners of the intense slow-transverse "diamond"; the left and right corners are more highly attenuated because Ω is larger for those directions. An additional comparison of theory and experiment for the deduced values of β is provided by Fig. 10.

It is possible to compute β using, for the dislocation density Λ, the values $\sim 3\times 10^7$ cm^{-2} and $\sim 2\times 10^8$ cm^{-2} for the 1.6% and 10% samples, respectively, as deduced from etch-pit counts on similar samples.[8] The computation gives $\beta \approx 7$ for the 1.6% sample, in excellent agreement with the value of $\beta \approx 7$ deduced from Fig. 12. For the 10% sample, however, the model of fluttering dislocations gives $\beta \approx 40$ which is a factor of 70 smaller that the value $\beta=2800$ deduced from our measurements using Fig. 12. In their application of the fluttering dislocation model to thermal conductivity data, Kneezel and Granato[14] concluded that a similar discrepancy for thermal conductivity is due to the existence of a high density of dislocation dipoles. They fitted the thermal conductivity data by assuming a dipole density of about 30 times the monopole density and an average spacing, between the two dislocations of the dipole pair, which is 60 times the Burgers vector. Dipoles are difficult to detect and would not be included in the etch-pit count utilized in our computation of β from the vibrating-string model. Although the frequency dependence of dipole scattering is different than that for monopoles, the anisotropy, again represented by the resolved shear-stress factor Ω, is the same as for monopoles. Hence the present analysis still applies. No dipole density is required to explain our results for the 1.6% sample but the dipole density for the 10% sample would be $\sim 10^{10}$ cm^{-2}.

Kneezel and Granato[14] also commented that the dislocations (or dipoles) should be fully pinned (see Sec. I) at a γ exposure of $\sim 2\times 10^5$ rad, which was believed to produce an average pinning-point separation L of $\sim 8\times 10^{-8}$ cm. However, Fig. 12 indicates that exposure to γ irradiation is still suppressing the phonon-dislocation interaction at an exposure of 6×10^6 rads, and that the reduction in β is roughly proportional to accumulated exposure between 6×10^5 and 6×10^6 rad. Even though this theoretical detail is not consistent with the present data, one should note that only the model of fluttering dislocations provides the highly anisotropic scattering that has been observed in the ballistic-phonon images.

As stated previously, the nonequivalence of the [010] and [001] directions indicated by the H/V ratio infers a strong predominance of the (110) and $(1\bar{1}0)$ glide-plane dislocations over the other possible $\{110\}$ systems. A quantitative analysis using computations similar to those described above indicates that, in the 10% sample, the β for the (110) slip-type dislocations must be at least 10^3 greater than the β for the (101) type. That is, the density of dislocations on the two slip planes shown in Fig. 2(a) is far greater than for other potential slip planes.

We had attempted to measure the frequency dependence of the phonon scattering. In the phonon-imaging experiment a Planck distribution of phonons, which may be characterized by a temperature T, is emitted by the heated metal film into the sample.[21,22] The temperature, and hence the average phonon frequency in the distribution, may be varied experimentally by changing the power density incident upon the metal film. This was done on the 1.6% sample by defocusing the laser, which provided a variation in metal-film temperature by about a factor of 3 from $T \approx 3$ K to $T \approx 10$ K. The measured H/V ratio remained constant $\sim \pm 3\%$, which suggests by Fig. 12 that β was constant to $\sim \pm 9\%$. This result seems to indicate that the scattering strength is only weakly frequency dependent above 3 K. The model, on the other hand, predicts β varying roughly as ω^{-n}, with $n \approx 1$ (unless the average of the dislocation resonant frequencies falls near the temperature range of our measurement). We cannot be certain whether this difference arises from a problem with the vibrating-string model, or because

the frequency distribution of phonons actually reaching the bolometer is not representative of that produced in the metal film.

A measurement of the Ninomiya resonance angle η_0, discussed after Eq. (3), is of interest because it would determine the ratio of the string tension to string mass, C/A, and would provide a value for the damping strength B. Unfortunately, the Ninomiya resonance could not be observed for our samples. There are several possible reasons for this. First, the resonance should be observable in the present experimental geometry only for screw dislocations. Thus the observed effect will be reduced by the ratio of the screw dislocation density to the edge dislocation density. Second, the (110) and (1$\bar{1}$0) slip systems would produce cancelling asymmetries if they were populated equally. That is probably not the case, though, since there was a clear rotation of the crystal [100] axis which favors the (110) slip plane. Third, the geometric asymmetry caused by the axis rotation of Fig. 2 prevents the assignment of the observed asymmetry along the horizontal ridge (Fig. 5) to the Ninomiya effect. Finally, the Ninomiya resonance would be attenuated by the presence of pinning points, being of little importance for phonons having a frequency ω near the fundamental dislocation resonance of $\sim\pi\bar{v}/L$.

IV. CONCLUSIONS

The scattering of thermal acoustic phonons from deformation-induced dislocations in LiF, as observed in a ballistic-phonon image, is strongly polarization dependent. The form of this anisotropic interaction agrees with that predicted by the theory of fluttering dislocations, which has the phonon scattered by sympathetic vibration of the dislocation. In a sample plastically deformed by 10% of its length and which has (110) and (1$\bar{1}$0) slip planes, a group of phonons (H) with wave vectors lying near the (001) plane transit the length of the sample ballistically. Another set (V), with wave vectors near the (010) plane, is partially transmitted. A comparison of these two intensities (H/V) gives, for the first time, a total scattering strength for dislocations. The resultant scattering strength, $\beta=2800$, implies that the most strongly scattered phonon polarizations have a mean free path of less than 10^{-3} of the sample length, or $l\lesssim 4\times 10^{-4}$ cm. This scattering strength is too strong to be explained theoretically by the observed density of isolated dislocations, and may indicate the participation of a larger density of dislocation dipoles. On the other hand, in a sample deformed by only 1.6%, the observed scattering strength is in good agreement with that calculated from the measured density of isolated dislocations.

The phonon-imaging technique has been shown to be a sensitive probe of defect scattering. The method yields details not available from thermal conductance measurements, especially when the phonon scattering is anisotropic. Phonon imaging provides a stringent test for models of phonon scattering. In the present work the scattering strength β, of the fluttering-string model, could be extracted because a selected population of dislocations was introduced by the deformation process. But even if the defects had been randomly oriented, the ratio of slow-transverse to fast-transverse scattering strengths would provide equivalent information.

ACKNOWLEDGMENTS

This work was supported by the National Science Foundation under the Materials Research Laboratory Grant No. DMR-80-20250 (G.A.N. and J.P.W.), and by the Department of Energy, Division of Materials Sciences, under contract No. DE-AC02-76ER01198 (E.J.C. and A.C.A.). The authors thank H. S. Ducoff for access to a Cs γ source.

[1]J. J. Gilman and W. G. Johnston, in *Solid State Physics*, edited by F. Seitz and D. Turnbull (Academic, New York, 1962), Vol. 13, p. 147; W. G. Johnston and J. J. Gilman, J. Appl. Phys. 30, 129 (1959).

[2]R. L. Sproull, M. Moss, and H. Weinstock, J. Appl. Phys. 30, 344 (1959).

[3]S. Ishioka and H. Suzuki, Proceedings of the International Conference on Crystal Lattice Defects, Kyoto, 1962 [J. Phys. Soc. Jpn. (Suppl. II) 18, 93 (1963)].

[4]A. Taylor, H. R. Albers, and R. O. Pohl, J. Appl. Phys. 36, 2270 (1965).

[5]M. Moss, J. Appl. Phys. 36, 3308 (1965).

[6]A. C. Anderson and M. E. Malinowski, Phys. Rev. B 5, 3199 (1972).

[7]E. P. Roth and A. C. Anderson, Phys. Rev. B 20, 768 (1979).

[8]E. J. Cotts, D. M. Miliotis, and A. C. Anderson, Phys. Rev. B 24, 7336 (1981).

[9]A condensed account of our work has been provided by G. A. Northrop, E. J. Cotts, A. C. Anderson, and J. P. Wolfe, Phys. Rev. Lett. 49, 54 (1982).

[10]For a brief description of the technique, see J. P. Wolfe,

Phys. Today 33 (12), 44 (1980).
[11]P. G. Klemens, in *Solid State Physics,* edited by D. Turnbull and F. Seitz (Academic, New York, 1958), Vol. 7, p. 1.
[12]Y. Kogure and Y. Hiki, J. Phys. Soc. Jpn. 38, 471 (1975).
[13]A. V. Granato, Phys. Rev. 111, 740 (1958).
[14]G. A. Kneezel and A. V. Granato, Phys. Rev. B 25, 2851 (1982); G. A. Kneezel, Ph.D. thesis, University of Illinois, 1980 (unpublished).
[15]G. A. Northrop and J. P. Wolfe, Phys. Rev. B 22, 6196 (1980); Phys. Rev. Lett. 43, 1424 (1979).
[16]G. A. Northrop, Ph.D. thesis, University of Illinois, 1982 (unpublished).
[17]M. T. Sprakling, *The Plastic Deformation of Simple Ionic Crystals* (Academic, New York, 1976).
[18]H. J. Maris, J. Acoust. Soc. Am. 50, 812 (1971).
[19]T. Ninomiya, J. Phys. Soc. Jpn. 25, 830 (1968).
[20]M. J. P. Musgrave, *Crystal Acoustics* (Holden-Day, San Francisco, 1970).
[21]O. Weis, Z. Angew. Phys. 26, 325 (1969).
[22]W. Kappus and O. Weis, J. Appl. Phys. 44, 1947 (1973).

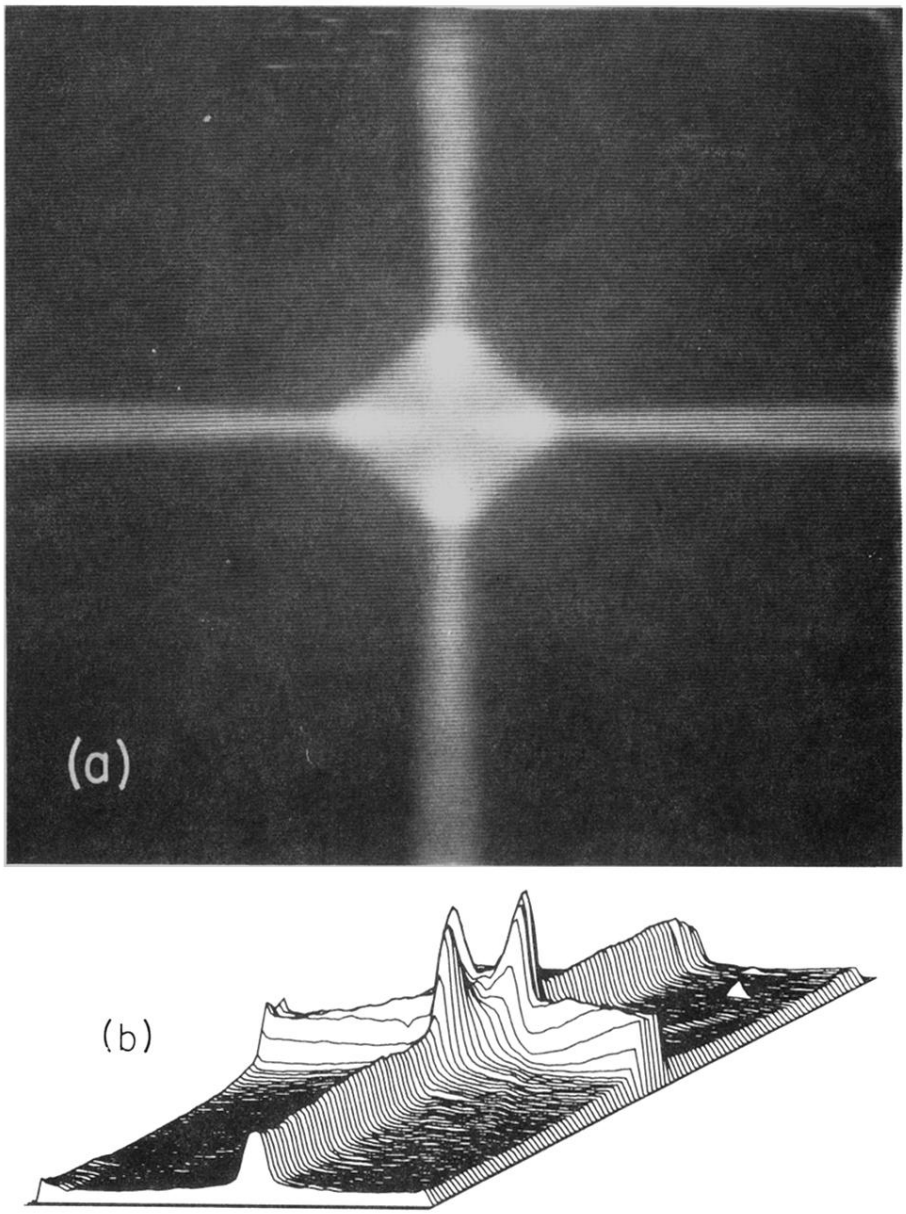

FIG. 3. (a) Ballistic-phonon image of the undeformed sample of LiF. The center corresponds to exact [100] propagation and the image extends to about 38° from the [100] axis at the edges. The brightness is proportional to the detected phonon intensity, and the anisotropy is due to phonon focusing. (b) Intensity profile of information in (a).

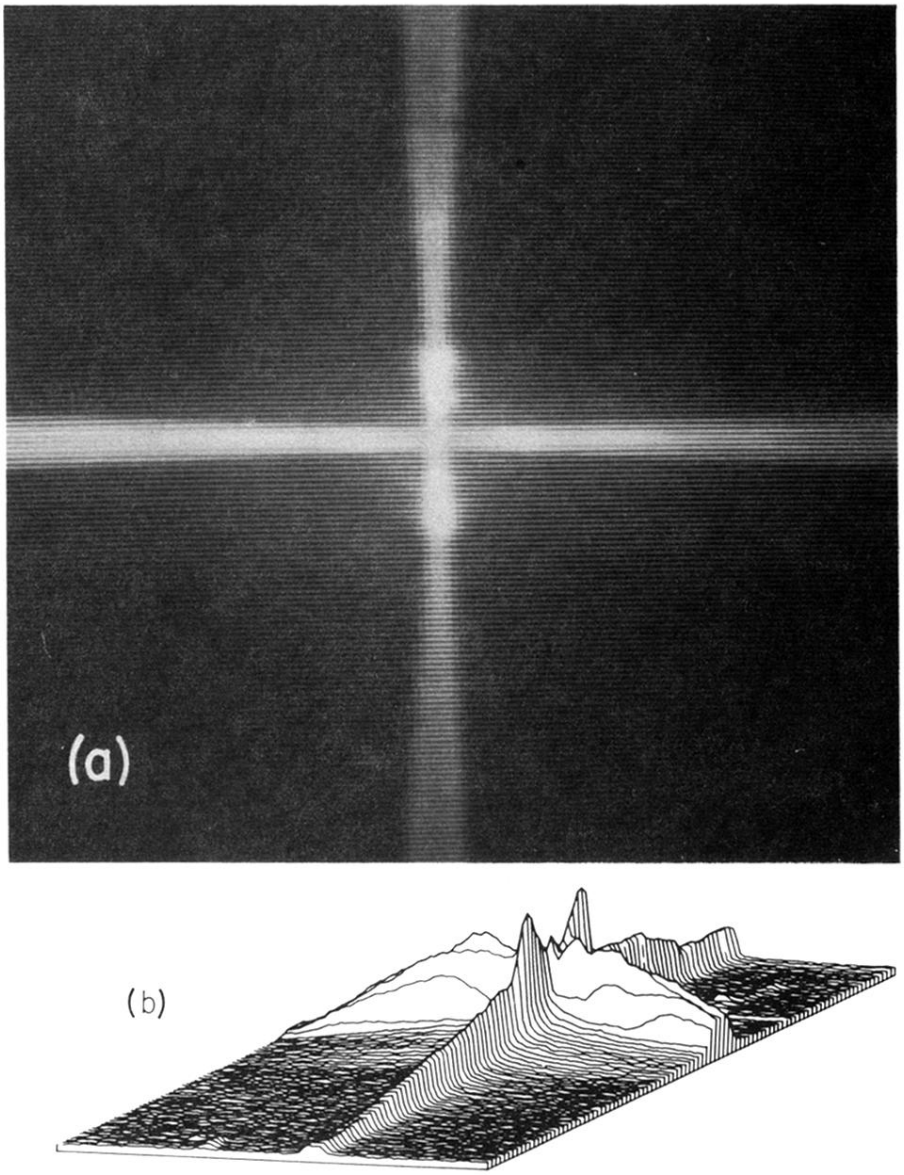

FIG. 4. (a) Ballistic-phonon image of the sample deformed by 1.6%. The viewing direction is along the direction of compression; the lateral expansion occurred in the horizontal direction in this figure. The intensity scale is arbitrary and cannot be compared directly with Figs. 3 or 5. (b) Intensity profile of information in (a).

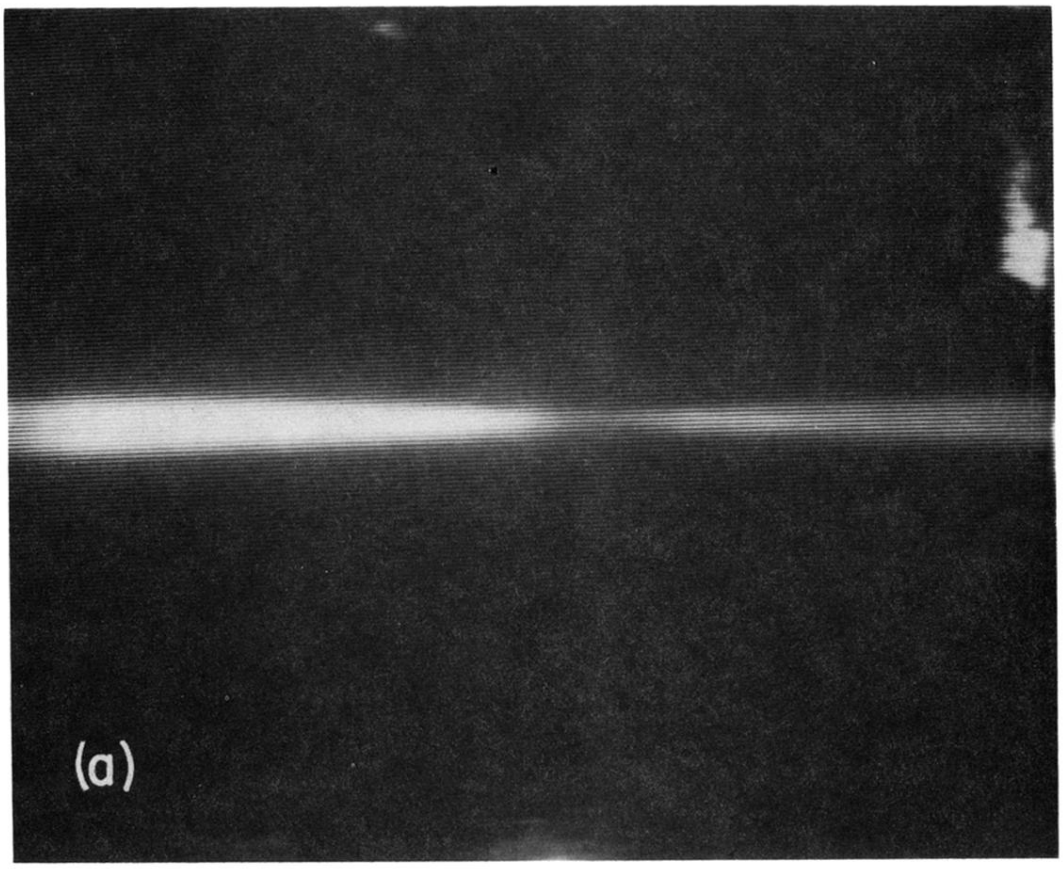

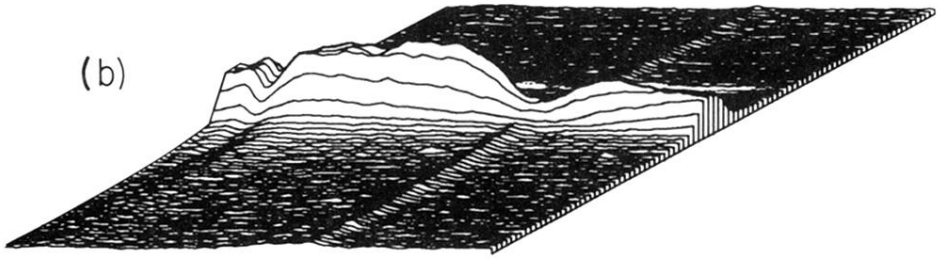

FIG. 5. Ballistic-phonon image of the sample deformed by 10%. Note the partial attenuation of the vertical ridge of the fast-transverse mode and the total attenuation of the slow-transverse mode. The dim vertical ridge may be difficult to see in (a), but it is evident in the intensity profile of (b). The fact that the intersection of the ridges is off center and that the horizontal ridge is most intense on the left is due to the reorientation of the [100] axis during deformation, as shown in Fig. 2(b). (The dip in intensity near the left end of the horizontal ridge is due to a defect in the constantan film.)

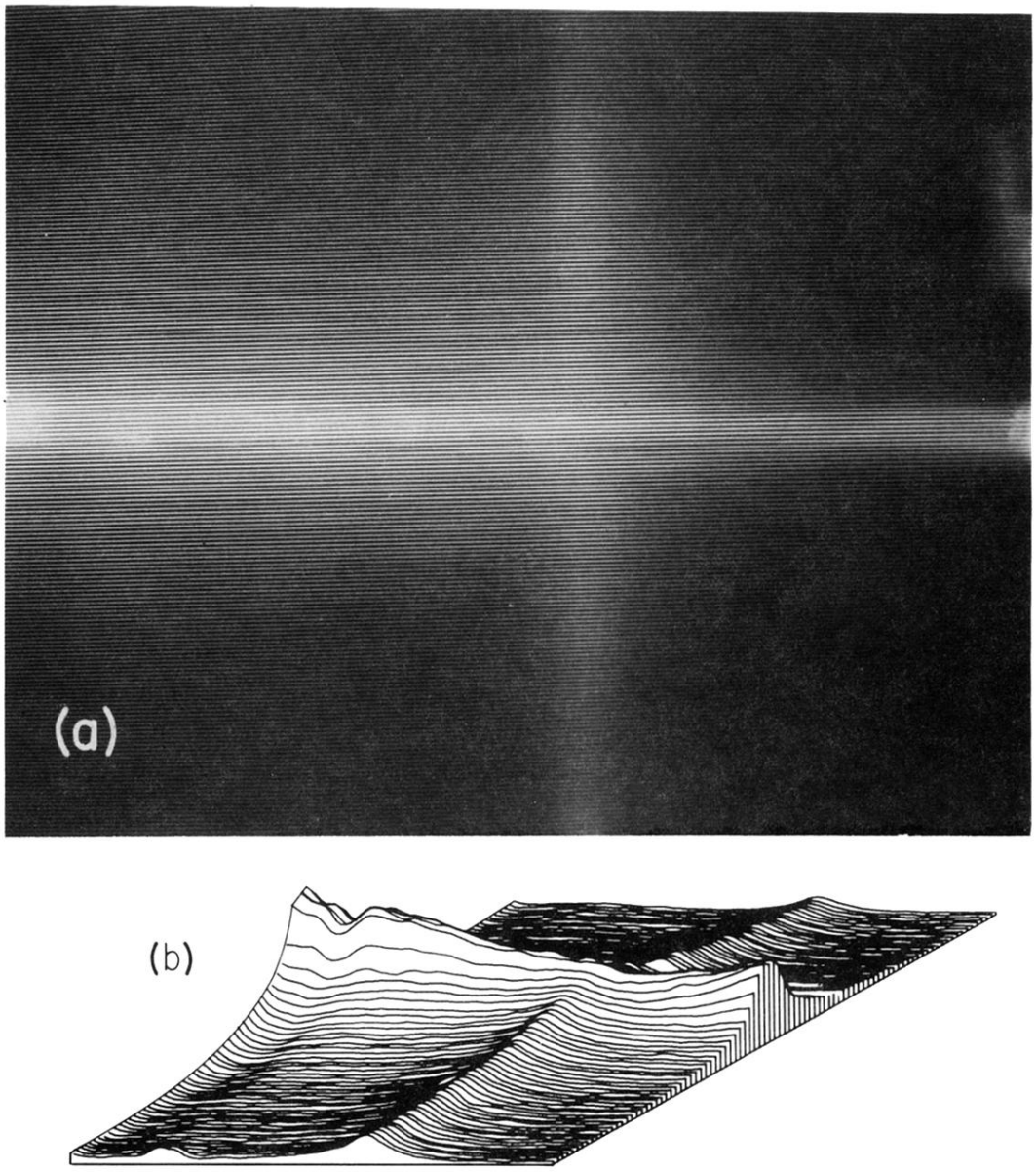

FIG. 6. Ballistic-phonon image (a) and intensity profile (b) of the 10% sample after exposure to 6×10^6 rad of γ irradiation. Note the increase in intensity of the vertical ridge relative to the horizontal ridge, compared to that in Fig. 5. Also the width of the ridge structure has increased due to scattering by defects introduced by γ irradiation.